# Supplementary Online Material

## RESYNCHRONIZATION DYNAMICS REVEAL THAT THE VENTRAL ENTRAINS THE DORSAL SUPRACHIASMATIC NUCLEUS

STEPHANIE R. TAYLOR, THOMAS J. WANG, DANIEL GRANADOS-FUENTES, AND ERIK D. HERZOG

## 1. Summary of Data Analysis

Below, we summarize the analyses of superpixels in 10 unilateral slices (Table S1) and of the cell-like regions of interest in the first 4 of those unilateral slices (Table S2).

Table S1. Summary of data from superpixel-based analysis of 5 SCN slices. For each of the clusters (ventral or dorsal) identified by the clustering analysis, we determined the mean (± std. dev.) period between 50 and 100 h after TTX treatment, the average synchronization index (SI) after the wash, the time to reach a stable period after the wash, the value of that stable period, and the difference in bioluminescence peak times between the two clusters.

| | | Period in TTX | Sync Index after wash | Time to stabilize | Stable period | Ventral peak time lead |
|---|---|---|---|---|---|---|
| Slice 1 (left) | Dorsal | 24.3 ±2.0 h | 0.96 | 96 h | 25.8 h | 3.0 h |
| | Ventral | 25.2 ±2.0 h | 0.95 | 82 h | 25.7 h | |
| Slice 1 (right) | Dorsal | 24.4 ±1.7 h | 0.96 | 87 h | 25.6 h | 2.7 h |
| | Ventral | 25.2 ±1.7 h | 0.97 | 41 h | 25.6 h | |
| Slice 2 (left) | Dorsal | 24.4 ±2.3 h | 0.91 | 99 h | 24.8 h | 3.2 h |
| | Ventral | 25.2 ±2.3 h | 0.97 | 73 h | 24.9 h | |
| Slice 2 (right) | Dorsal | 24.6 ±2.1 h | 0.94 | 106 h | 25.0 h | 3.0 h |
| | Ventral | 25.3 ±2.4 h | 0.96 | 70 h | 25.0 h | |
| Slice 3 (left) | Dorsal | 23.7 ±2.1 h | 0.95 | 115 h | 24.7 h | 3.8 h |
| | Ventral | 25.1 ±2.1 h | 0.97 | 36 h | 24.8 h | |
| Slice 3 (right) | Dorsal | 23.7 ±2.2 h | 0.94 | 86 h | 24.9 h | 1.6 h |
| | Ventral | 24.7 ±2.5 h | 0.96 | 36 h | 24.8 h | |
| Slice 4 (left) | Dorsal | 25.1 ±0.9 h | 0.95 | 107 h | 24.9 h | 1.7 h |
| | Ventral | 25.2 ±0.7 h | 0.98 | 101 h | 24.8 h | |
| Slice 4 (right) | Dorsal | 25.1 ±0.7 h | 0.95 | 107 h | 25.0 h | 2.0 h |
| | Ventral | 25.2 ±0.6 h | 0.97 | 101 h | 24.8 h | |
| Slice 5 (left) | Dorsal | 24.1 ±0.6 h | 0.98 | 75 h | 24.6 h | 1.2 h |
| | Ventral | 24.6 ±0.5 h | 0.98 | 36 h | 24.6 h | |
| Slice 5 (right) | Dorsal | 24.3 ±0.5 h | 0.96 | 108 h | 24.5 h | 1.3 h |
| | Ventral | 24.6 ±0.4 h | 0.98 | 109 h | 24.3 h | |

TABLE S2. Summary of data from ROI-based analysis of 2 SCN slices. For each of the clusters (ventral or dorsal) identified by the clustering analysis, we determined the mean (± std. dev.) period between 50 and 100 h after TTX treatment, the average synchronization index (SI) after the wash, the time to reach a stable period after the wash, the value of that stable period, and the difference in bioluminescence peak times between the two clusters.

| | | Period in TTX | Sync Index after wash | Time to stabilize | Stable period | Ventral peak time lead |
|---|---|---|---|---|---|---|
| Slice 1 (left) | Dorsal | 24.7 ± 1.9 h | 0.94 | 97 h | 25.2 h | 3 h |
| | Ventral | 25.1 ± 2.1 h | 0.97 | 62 h | 24.9 h | |
| Slice 1 (right) | Dorsal | 24.8 ± 1.8 h | 0.96 | 109 h | 25.0 h | 3 h |
| | Ventral | 25.1 ± 1.9 h | 0.97 | 66 h | 25.0 h | |
| Slice 2 (left) | Dorsal | 23.9 ± 1.8 h | 0.96 | 102 h | 25.8 h | 3 h |
| | Ventral | 25.2 ± 1.4 h | 0.96 | 84 h | 25.6 h | |
| Slice 2 (right) | Dorsal | 24.0 ± 1.2 h | 0.97 | 90 h | 25.5 h | 3 h |
| | Ventral | 25.2 ± 1.3 h | 0.97 | 37 h | 25.6 h | |

## Analyzing Spatial Patterns

We performed additional analyses using more than two clusters. Here we describe how we quantify the patterns.

**Methods.** SPATIAL ARRANGEMENT OF CLUSTERS. To determine the spatial pattern of the clusters, we first characterized each cluster by its distance $d$ (mean distance from the ventrolateral or central point) and its dynamic characteristic (mean peak time or amplitude). We then grouped the set of ($d$, dynamic characteristic) points for a given set of clusters into a *pattern summary* (e.g. for an analysis of the base condition with $k = 3$, there will be three points). If a spatial pattern were present, we would expect points in a pattern summary to be linear and for the distances to cover a wide range. An ideal pattern would have k evenly spaced points and would therefore cover a range of $1 - \frac{1}{k}$. If a spatial pattern were not present, we would expect all distances to be similar and for the range to be small. We therefore computed the Pearson correlation coefficient to determine linearity and then quantified the spatial coverage of the pattern as the fraction of the ideal range covered by the distances.

$$\text{coverage} = \frac{\Delta d}{D} / \left(1 - \frac{1}{k}\right)$$

where $\Delta d$ is the difference between the maximum and minimum distances and $D$ is the maximum possible distance from the ventrolateral or central point. An ideally clear pattern will have a coverage of unity and a completely amorphous pattern will have a coverage of zero.

SIMILARITY OF CLUSTER SPATIAL PATTERNS. We quantified the similarity of spatial patterns across the experimental conditions by determining the distance between the pattern summaries for a given value of k. We defined the distance between two pattern summaries as the average Euclidean distance between pairs of points in the corresponding clusters. For example, with amplitude-based clustering, this meant comparing the (distance, amplitude) point in the lowest-amplitude cluster during one condition to the (distance, amplitude) point in the lowest-amplitude cluster.

**Results.** For a representative unilateral slice, we computed up to 5 clusters using both the correlation distance (phase-based clustering) and the Euclidean distance (amplitude-based clustering) (Figure S2) and computed the pattern summaries. We then examined the set of pairs (each line in Figure S3) from each clustering analysis. Those with a clear spatial ordering were linear (Pearson's $R^2 > 0.8$) and were spatially spread apart (with somewhat clear patterns having a coverage measure $> 0.2$ and clear patterns having a coverage measure $> 0.5$). For amplitude-based clustering, the pattern was somewhat clear before TTX, lost amplitude, but not clarity, during TTX treatment, and regained some, but not all, amplitude after removal of TTX. For phase-based clustering, the pattern was clear before TTX, became unclear during TTX treatment, and recovered after TTX treatment. We verified the recovery of the phase pattern by comparing patterns across experimental conditions. The difference between the patterns for the pre-TTX and TTX conditions

was more than twice the difference between the patterns for the pre-TTX and post-TTX conditions. This indicated that resynchronization dynamics recovered the spatial pattern of an unperturbed slice, even at the more fine-grained scale. However, using the fine-grained scale did not improve the similarity of patterns.

## 2. Introduction to Mathematical Model

We designed an ordinary differential equation (ODE) model of the population of oscillators in the SCN. We simulated the model (numerically solved the ODE's using Matlab's ode15s) under a carefully selected set of configurations (including network topology and connectivity between regions) to determine that the configuration that best explains the slice data is one in which the core sends signals to the shell. We describe the model in Section 3 and provide details about the configurations in Section 4.

## 3. Mathematical Model

The mathematical model captures the phase and amplitude of oscillation of each oscillator in a network of oscillators. The basic components of the model include:

- The phase and amplitude of each oscillator,
- Intercellular signaling using a given network topology, and
- Phase and amplitude adjustments that individual cells make in response to intercellular signaling.

For the clock in each cell, the model is a generic 2D limit cycle oscillator in polar coordinates with two key additions: 1) the amplitude affects the phase response and 2) the amplitude increases in response to the signal.

$$\frac{d\theta_i}{dt} = 1 + \mathrm{VRC}(\theta_i(t), A_i(t), A_i^0, \tau_i, \vec{p})\frac{\gamma_i(\vec{\theta}, \vec{A}, \vec{\tau}, \delta, \mathbf{N})}{\gamma_i(\vec{\theta}, \vec{A}, \vec{\tau}, \delta, \mathbf{N}) + K} \tag{1}$$

$$\frac{dA_i}{dt} = -\lambda(A_i(t) - A_i^0) + \kappa\frac{\gamma_i(\vec{\theta}, \vec{A}, \vec{\tau}, \delta, \mathbf{N})}{\gamma_i(\vec{\theta}, \vec{A}, \vec{\tau}, \delta, \mathbf{N}) + K} \tag{2}$$

where $\theta_i(t)$ is the phase at time $t$ (in hours), $A_i(t)$ is the amplitude (in a.u.) at time $t$. Their dynamics depend on a velocity response curve (VRC), the concentration $\gamma_i$ of the signaling agent at cell $i$'s receptors (i.e, the signal), the cell amplitude's decay rate $\lambda$, and the cell amplitude's growth rate $\kappa$. The concentration of the signal saturates with an activation threshold $K$. The VRC is a function of the phase, the current amplitude, the steady-state amplitude $A_i^0$, the cell's intrinsic period $\tau_i$, and a set of parameters $\vec{p}$ that determine its shape and magnitude. The signal input depends on the vector $\vec{\theta}$ of phases for all cells, the vector $\vec{A}$ of amplitudes for all cells, the vector $\vec{\tau}$ of intrinsic periods for all cells, a phase offset $\delta$ determining when the signal peaks, and the adjacency matrix $\mathbf{N}$ for the signaling network.

3.1. **VRC.** The VRC's shape is determined by the parameters $\vec{p}$ and the phase $\vec{\theta}$ and intrinsic period $\tau$ determine the value of the VRC at that moment. The value is scaled by a function of the the amplitude, such that the phase velocity response will be smaller if the current amplitude is larger.

$$\mathrm{VRC}(\theta, A, A^0, \tau, \vec{p}) = e^{A^0 - A}v(\theta, \tau, \vec{p})$$

where $v$ is a function composed of several smooth step-like pieces, depending upon the region of the VRC. The VRC has a dead zone, a delay zone, and an advance zone. The step pieces are from the end of the deadzone down to the trough of the delay zone, from the trough of the delay zone up to the peak of the advance zone, and from the peak of the advance zone to the beginning of the deadzone in the next cycle. The entries in $\vec{p}$ determine the beginning and end phase of each region, as well as its magnitude. The entries of $\vec{p}$ in order are:

- $\phi_{\text{dz0}}$: the phase at which the deadzone begins (CT)
- $\phi_{\text{dz1}}$: the phase at which the deadzone ends (CT)
- $\phi_{\text{trough}}$: the phase of the VRC's trough (CT)
- trough: the magnitude of it trough (a.u.)
- $\phi_{\text{peak}}$: the phase of the VRC's peak (CT)
- peak: the magnitude of it peak (a.u.)

The function $v(\theta, \tau, \vec{p})$ is defined as

$$v(\theta,\tau,\vec{p}) = \begin{cases} 0, & \text{if } \phi_{dz0} \le \phi < \phi_{\text{dz1}} \\ s(\phi, \phi_{\text{dz1}}, 0, \phi_{\text{trough}}, \text{trough}), & \text{if } \phi_{\text{dz1}} \le \phi < \phi_{\text{trough}} \\ s(\phi, \phi_{\text{trough}}, \text{trough}, \phi_{\text{peak}}, \text{peak}), & \text{if } \phi_{\text{trough}} \le \phi < \phi_{\text{peak}} \\ s(\phi, \phi_{\text{peak}}, \text{peak}, 24 + \phi_{dz0}, 0), & \text{otherwise} \end{cases}$$

where $\phi$ is the phase in circadian time, shifted to be in the range from the beginning of the deadzone in one cycle to the beginning of the deadzone in the next cycle. It is computed as

$$\phi = \begin{cases} \hat{\phi}, & \hat{\phi} \ge \phi_{dz0} \\ 24 + \hat{\phi}, & \text{otherwise} \end{cases}$$

where $\hat{\phi} = (\theta \frac{24}{\tau} \mod 24)$.

$s$ is a function that produces either a step-like slope up or a step-like slope down, with the steepness of the slope dependent upon the width of the piece. $s$ evaluated at either the beginning or end of the region has a slope of 0, making it possible to attach pieces to each other and to horizontal lines such that the resulting piece-wise polynomial is continuous and further that its first derivative (with respect to phase) is continuous.

$$s(\phi, \phi_0, y_0, \phi_1, y_1) = \begin{cases} y_0 + \Delta y, & \text{if } y_0 < y_1 \\ y_0 - \Delta y, & \text{otherwise} \end{cases}$$

where

$$\Delta y = \frac{\frac{1}{6}\phi^3 - \frac{\phi_0+\phi_1}{4}\phi^2 + \frac{\phi_0\phi_1}{2}\phi + \frac{\phi_0^3}{12} - \frac{\phi_0^2\phi_1}{4}}{-\frac{\phi_1^3}{12} + \frac{\phi_0\phi_1^2}{4} - \frac{\phi_0^2\phi_1}{4} + \frac{\phi_0^3}{12}} |y_1 - y_0|$$

and $\phi$ is the phase at which the step's value should be evaluated. The step begins at phase $\phi_0$ with the value $y_0$ and ends at phase $\phi_1$ with the value $y_1$.

3.2. **Intercellular signaling.** The signal input to the $i^{th}$ cell is the average of the weighted outputs of all cells that send signals to it. The entries in $N$ determine those weights. $N_{j,i}$ is the weight of the signal sent from cell $j$ to cell $i$.

$$\gamma_i(\vec{\theta}, \vec{A}, \vec{\tau}, \delta, \mathbf{N}) = \begin{cases} \frac{\langle \vec{o}, N_{*,i} \rangle}{\text{count}(N_{*,i})}, & \text{there is at least one nonzero entry in } N_{*,i} \\ 0, & \text{otherwise} \end{cases}$$

where the signal output of all cells is the vector $\vec{o}$, $\langle \cdot, \cdot \rangle$ is the standard inner product, and $\text{count}(N_{*,i})$ is the number of nonzero entries in the $i^{th}$ row of the network's adjacency matrix.

The signal output of the $j^{th}$ cell is

$$o_j(\theta_j, A_j, \tau_j, \delta) = 0.7 \left( \frac{A_j}{2} \sin\left( (\theta_j - \delta) \frac{2\pi}{\tau_j} \right) + \frac{A_j}{2} \right).$$

3.3. **Estimating *per* mRNA.** To compare simulation output to experimental data, we need a trace over time of the bioluminescence for each cell. To do so, we estimate the *per* mRNA (MP) levels as a sine curve. Given the intrinsic period $\tau$ and values of phase and amplitude at a given time $t$, the *per* mRNA level is

$$\text{MP}(t) = \frac{A(t)}{2} \sin\left( \theta(t) \frac{2\pi}{\tau} \right) + \frac{A(t)}{2} \tag{3}$$

3.4. **Parameter-Fitting.** Our goal was to find values for the VRC parameters that would allow model simulations to capture the following characteristics:

- The core and shell are subnetworks with a few connections between them.
- The core and shell cells have intrinsic period distributions taken from experimental results (core cells have longer periods than shell cells, and they each follow a Gaussian distribution with a standard deviation of approximately 1.5 h) and synchronize with a period reflecting experimental results (the period is approximately 25.5 h).

We sampled 194 VRC shape parameter sets from a space with bounds that reflect the variety of VRC's we have computed from mechanistic models. For each of the parameter sets, we multiplied the trough and peak values by 5 different possible scales, leading to 970 different VRC's. The range for each parameter value is shown in Table S3.

For each of the 970 VRC's, we constructed a system of ordinary differential equations, using Eqs. 1 and 2. The details follow:

- We constructed a network with 169 core shells laid out in a 13 × 13 grid and 169 shell cells also laid out in a 13 × 13 grid. The core cells were connected via a nearest neighbor network with additional, random (potentially long-range) connections (for pair of cells, the probability that they were connected was 5%). The shell cells were connected via a nearest neighbor network (each cell was connected to the neighbor directly above, below, to the left, and to the right of it). The core and shell were connected such that every core cell received a signal from exactly one (randomly

chosen) shell cell and every shell cell received a signal from exactly one (randomly chosen) core cell.
- Every cell used a set of parameters that were fixed for all simulations (see Table S4).
- Each core cell was given an intrinsic period chosen from a Gaussian distribution with mean 25.1 h and standard deviation 1.3 h, and each shell cell was given an intrinsic period chosen from a Gaussian distribution with mean 23.9 h and standard deviation 1.9 h. These distributions are representative of the distribution of periods during TTX.

For each of these sets of ODE's, we carried out simulations for each of 11 values of $\delta$ (evenly spaced values ranging from -4 to -2).

- To simulate the network transitioning from asynchrony to synchrony in constant darkness, we used Matlab's ode15s ODE solver, beginning with each cell at a randomly chosen phase and an initial amplitude of 1, running the simulation for 360 (simulated) hours.
- We then tested the simulation to see if it met certain criteria:
  - The simulated cells reached a stable period (the standard deviation of the cycle-to-cycle differences for the last 5 cycles is less than 0.1 h).
  - The stable period reached by the cells is within 1.5 h of 25.5 h.
  - The peak of the average core *per* mRNA trace (computed according to Eq. 3) is between 0 and 6 h after the peak of the average shell *per* mRNA trace.
- If the simulation met the above criteria, we then tested the ability of the model to be entrained to a light/dark cycle. We modeled light as an additive value to $\gamma_i$ for each core cell (light adds 5.5 a.u. to $\gamma$ for the first hour of each day and 1.1 a.u. for the remaining 11 hours). We simulated 6 24-hours days with 12 hour photoperiods (LD12:12), testing whether or not the model cells would entrain by the end of the simulation. If it entrained, we labeled the simulation as "working".

Of these 10,670 simulations, 83 yielded the desired output. The range of $\delta$ values for the 83 working simulations was the same as the range originally sampled. The range of VRC parameter values for the 83 working simulations is shown in Table S5.

## 4. Simulation configurations and details

We sought to determine whether or not the experiment results indicated that connections from the core to the shell were stronger than the reverse connections. We ran a set of simulations using the 83 working VRC-$\delta$ pairs identified above. For each pair, we simulated the model using one of 1320 configurations. The configurations were determined by

- the strength and number of the connections from the core to the shell,
- the strength and number of the connections from the shell to the core,
- the network topology for the core,
- the network topology for the shell, and
- the distributions of intrinsic periods.

Each simulation mimicked the wash condition of the TTX experiments:

- We simulated 360 h of recovery from TTX.
- The initial values of the phase for each cell were chosen from a random uniform distribution in the range of 0 to 24 (to indicate the asynchrony in TTX).
- The initial values of the amplitudes for each were 1 (to indicate how weak the cells become in TTX).

For each simulation, we computed *per* mRNA traces from the phase and amplitude outputs and used them to measure

- the period of the cells, once it had stabilized (computed as the mean period of all cells in the region between hours 240 and 350),
- the number of hours it took for the core cells to reach a stable period (i.e. to remain within 0.1 h of the stable period),
- the number of hours it took for the shell cells to reach a stable period (i.e. to remain within 0.1 h of the stable period),
- the average synchronization index over the entire simulation, and
- the difference in peak time between the core and shell (i.e. the difference in timing between the final peak of mean core *per* mRNA trace and the mean shell *per* mRNA trace).

4.0.1. *Connections between regions.* We varied the strength of the inter-regional connections such that the overall directionality of the signals would transition from purely core-to-shell, to equal in both directions, to purely shell-to-core. We increased weight of the connections from the shell to the core from 0 to 1 (while holding the shell-to-core strength at 1), then decreased weight of the connections from the core to the shell from 1 to 0 (while holding the shell-to-core strength at 1) (see Table S6).

Additionally, we varied the number of connections between the core and shell. We used the same process for connecting the regions as described above, but allowed for any number of connections between the regions. For a given number of connections ($M$=1, 2, 3, 4, or 5) we generated the inter-region connections thus: for each cell in the core, we randomly chose $M$ cells in the shell to send signals to it and, for each cell in the shell, we randomly chose $M$ cells in the core to send signals to it.

4.0.2. *Network topology within a region.* We used the regional topologies described above: a) nearest-neighbor (NN) and b) nearest-neighbor with additional random connection (NN+R). We tested configurations that allowed one or both regions to use a NN+R topology (see Table S7). We did not use NN for both regions because that configure did not allow the model to synchronize.

4.0.3. *Period distributions.* We generated four populations, each with a subpopulation of slower cells and a subpopulation of faster cells (see Table S8). Each population was used for two configurations – one with the fast period in the core and one with the slow periods in the core.

TABLE S3. Search space for VRC parameters

| VRC Shape Parameter | Range of Values |
|---|---|
| $\phi_{dz0}$ | CT5 to CT5.3 |
| $\phi_{dz1}$ | CT5.4 to CT10.7 |
| $\phi_{\text{trough}}$ | CT7.8 to CT16 |
| trough | -54 (1/a.u.) to -12.6 (1/a.u.) |
| $\phi_{\text{peak}}$ | CT22 to CT24 and CT0 to CT3.8 |
| peak | 14 (1/a.u.) to 81 (1/a.u.) |

TABLE S4. Parameter values fixed for all simulations

| Parameter | Value |
|---|---|
| $\lambda$ | 0.1 ($h^{-1}$) |
| $K$ | 10.0 (a.u.) |
| $\kappa$ | 1.5 (a.u./h) |
| $A^0$ | 1 (a.u.) |

TABLE S5. Range of VRC parameters in working simulations

| VRC Shape Parameter | Range of Values |
|---|---|
| $\phi_{dz0}$ | CT5 to CT5.3 |
| $\phi_{dz1}$ | CT5.7 to CT7.7 |
| $\phi_{\text{trough}}$ | CT8.9 to CT13.5 |
| trough | -45.8 (1/a.u.) to -20.5 (1/a.u.) |
| $\phi_{\text{peak}}$ | CT22 to CT24 and CT0 to CT3 |
| peak | 31.5 (1/a.u.) to 70.2 (1/a.u.) |

TABLE S6. Weights of edges in network

| Strength Configuration | 1 | 2 | 3 | 4 | 5 | 6 | 7 | 8 | 9 | 10 | 11 |
|---|---|---|---|---|---|---|---|---|---|---|---|
| Within core | 1 | 1 | 1 | 1 | 1 | 1 | 1 | 1 | 1 | 1 | 1 |
| Within shell | 1 | 1 | 1 | 1 | 1 | 1 | 1 | 1 | 1 | 1 | 1 |
| Core to shell | 1 | 1 | 1 | 1 | 1 | 1 | 0.8 | 0.6 | 0.4 | 0.2 | 0 |
| Shell to core | 0 | 0.2 | 0.4 | 0.6 | 0.8 | 1 | 1 | 1 | 1 | 1 | 1 |

TABLE S7. Regional network topologies used in simulations

| | Core | Shell |
|---|---|---|
| Network Configuration 1 | NN+R | NN |
| Network Configuration 2 | NN | NN+R |
| Network Configuration 3 | NN+R | NN+R |

TABLE S8. Mean ± standard deviations (h) of Gaussian distributions used to generate intrinsic periods

| | Slow | Fast | Reason |
|---|---|---|---|
| Population 1 | 25.1 ± 1.6 | 24.3 ± 1.69 | To test the average population from the slices |
| Population 2 | 25.2 ± 1.27 | 24 ± 1.24 | To test a representative population |
| Population 3 | 25 ± 1.95 | 24.5 ± 1.97 | To test a representative population with a large range of periods |
| Population 4 | 25 ± 1.25 | 24.5 ± 1.25 | To test population 3 with a smaller range of periods |

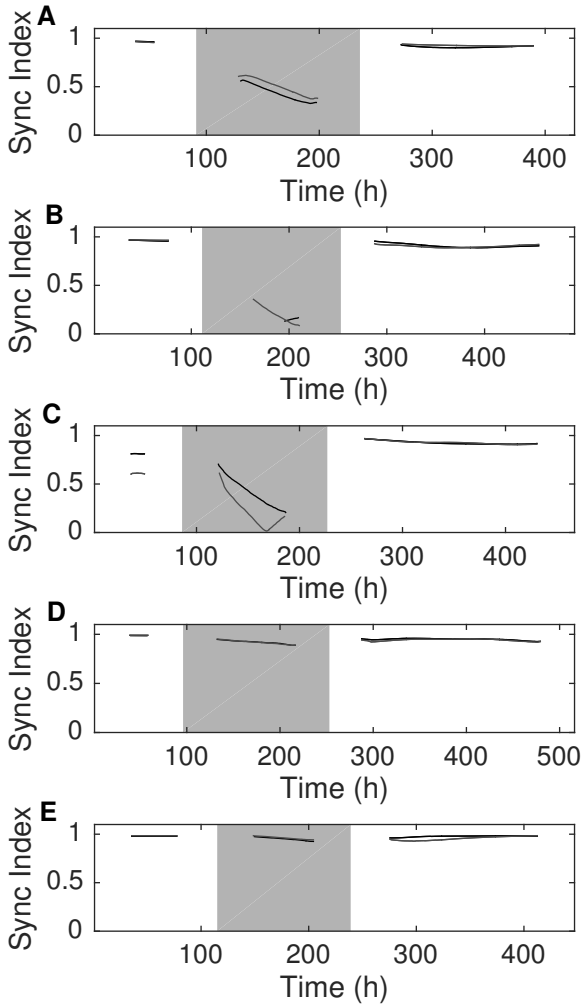


FIGURE S1. **Recordings from 5 representative bilateral SCN reveal that synchrony among circadian cells was reliably reduced during 6 days of TTX treatment and recovered after removal of the TTX.** We show the synchronization index for the left (black) and right lobes (gray) from 5 slices each recorded for over 17 days (A-E).

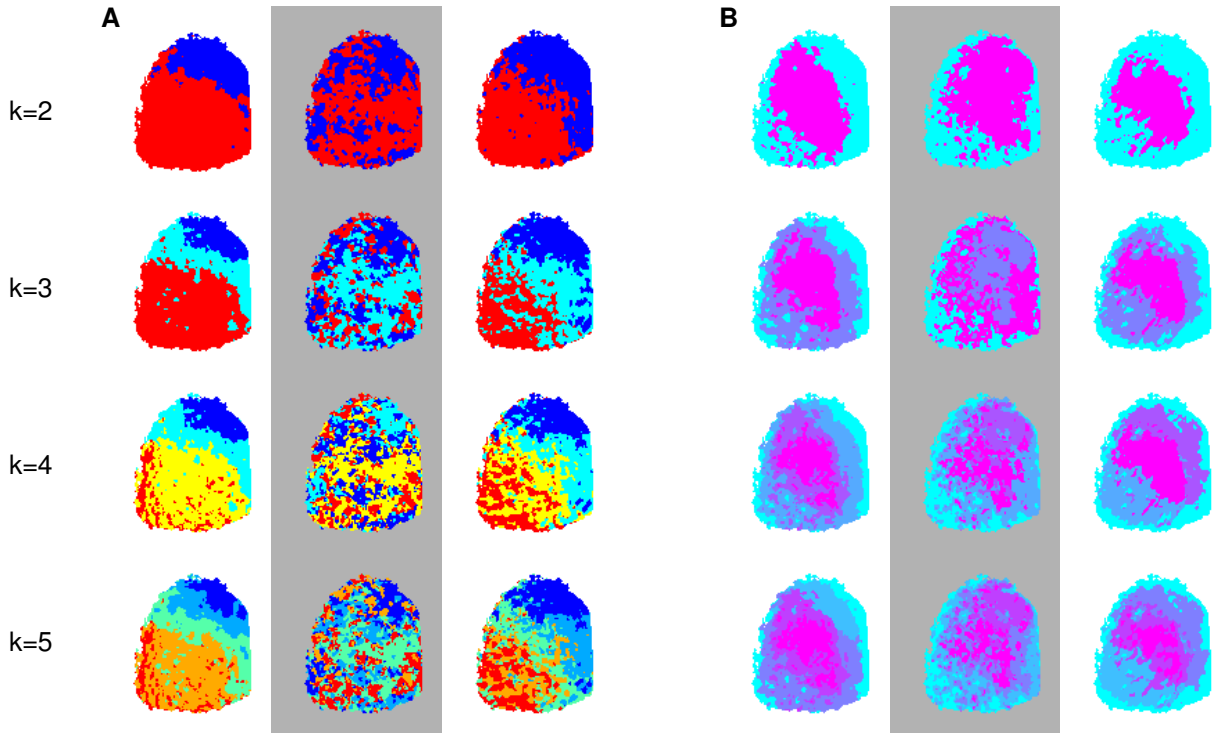


FIGURE S2. **Clustering analyses identified spatial patterns in phase and amplitude that were restored when TTX was washed out.** Shown are the results of k-means clustering analyses of the traces from a representative unilateral SCN before, during and after TTX as in Figure 1C and D. Here, we compare results as a function of the number of clusters sought (k). A) The clustering algorithm uses the correlation distance measure and the clusters are colored according to the average peak time of their final peak. The colors range from blue (earliest peaks) through the rainbow to red (latest peaks). B) The clustering algorithm uses the squared Euclidean distance measure and the clusters are colored according to their mean amplitudes ranging from magenta (high amplitude) to purple to blue to cyan (low amplitude). Note that SCN cells could be reliably grouped into spatially distinct core and shell regions by their similar time and amplitude of peak PER2 express before and after TTX treatment. In contrast, these spatial groupings, especially the phasing of PER2, were disrupted during days 3-6 of TTX treatment.

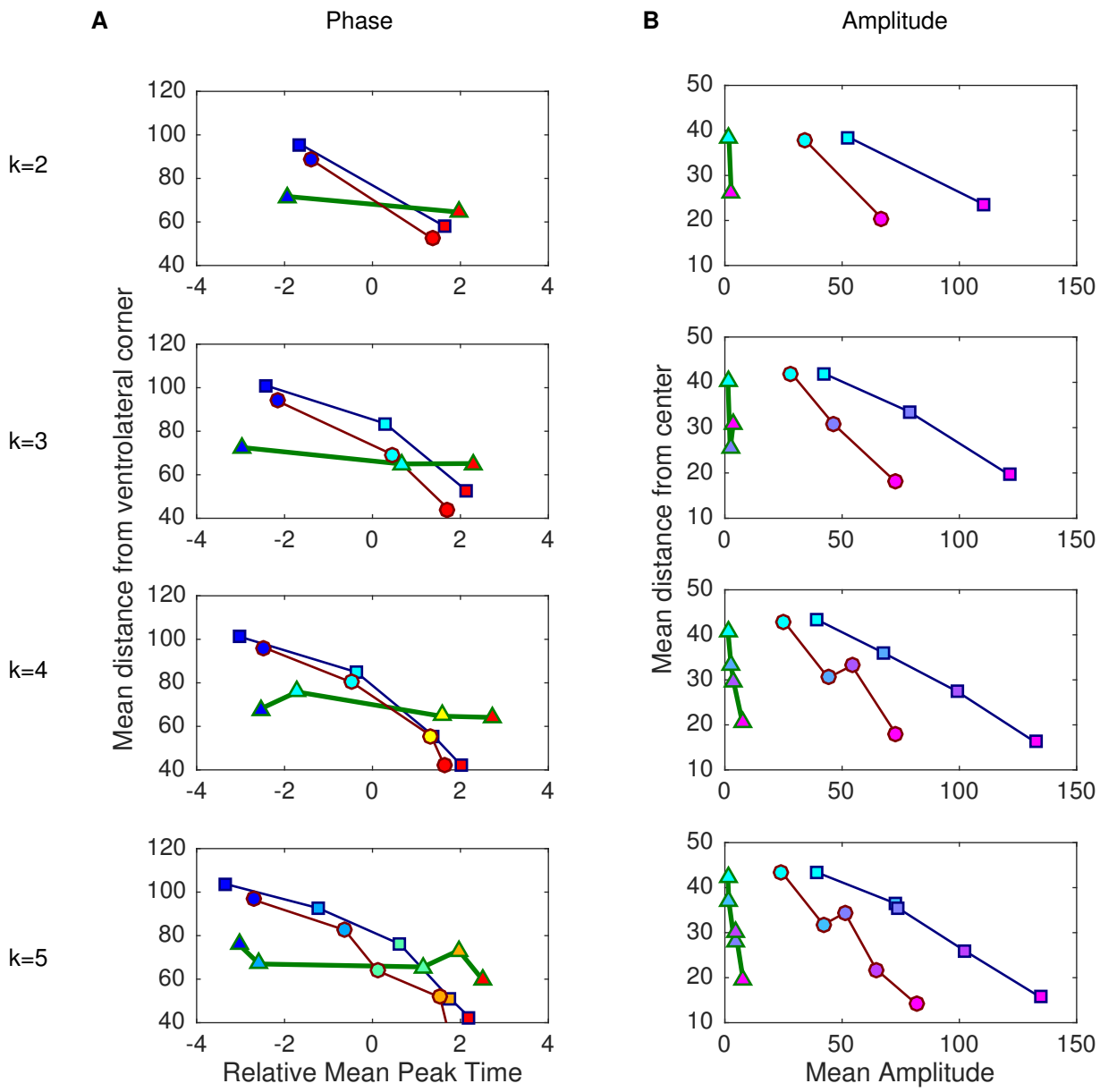


FIGURE S3. **Spatial patterns in phase were destroyed by TTX and restored when TTX was removed.** K-means clustering of a representative unilateral SCN shows that during TTX (triangles, thick green line), the relative times of peak PER2 (A) and mean amplitude (B) for each identified cluster (each color represents cells with similar phase or amplitudes, respectively) differed compared to before (squares, blue line) and after TTX (squares, red line). (A) Phase analysis led to clusters that were characterized by their mean relative peak time and by the mean distance of the pixels in a given cluster to the ventrolateral corner of the SCN slice. (B) Amplitude analysis led to clusters that were characterized by their mean amplitudes and by the mean distance of the superpixels in a given cluster to the center of the slice. Note that the phase and amplitude clusters were most similar to each other before and after TTX and that addition of more than two clusters did not improve the similarity of these groups before and after TTX treatment.

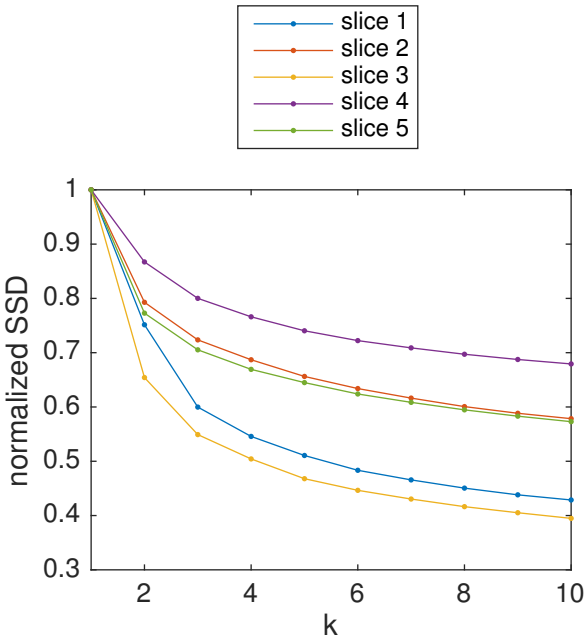


FIGURE S4. **The SCN can be clustered into two groups with little gained by increasing the number of clusters (k).** For each of the 5 bilateral SCN recorded, we computed the sum of the squared correlation distances (SSD) from each point to the center of its cluster. This distance (shown here normalized to the value when k=1) decreased dramatically for 2 clusters and then modestly declined for analyses seeking between 3 to 10 clusters within each SCN.

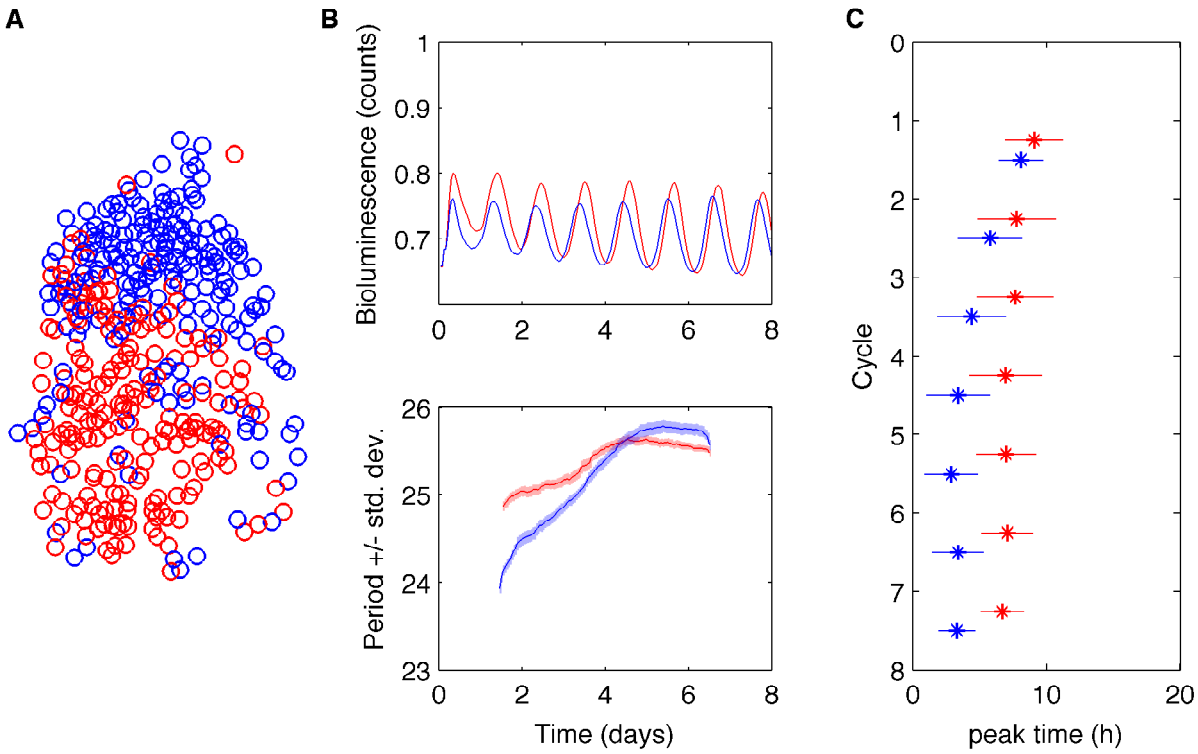


FIGURE S5. **Cell-based clustering reveals that, following removal of TTX, the dorsal region attained a stable period after the ventral region and established an earlier time of peak PER2 expression.** A) Shown are the cells in the left lobe of SCN 2, color-coded by cluster. B) The mean PER2 expression (top) and period (SEM) of neurons in each cluster. Similar to the results of automated superpixel-based analysis (Figure 2), the neurons in the red cluster reached their stable period sooner. The cumulative PER2 expression of neurons in the blue cluster increased in amplitude. C) The mean time of daily peak PER2 expression (+/- SD) for the blue cluster reached a steady state of about 3 h earlier than for cells in the red cluster.

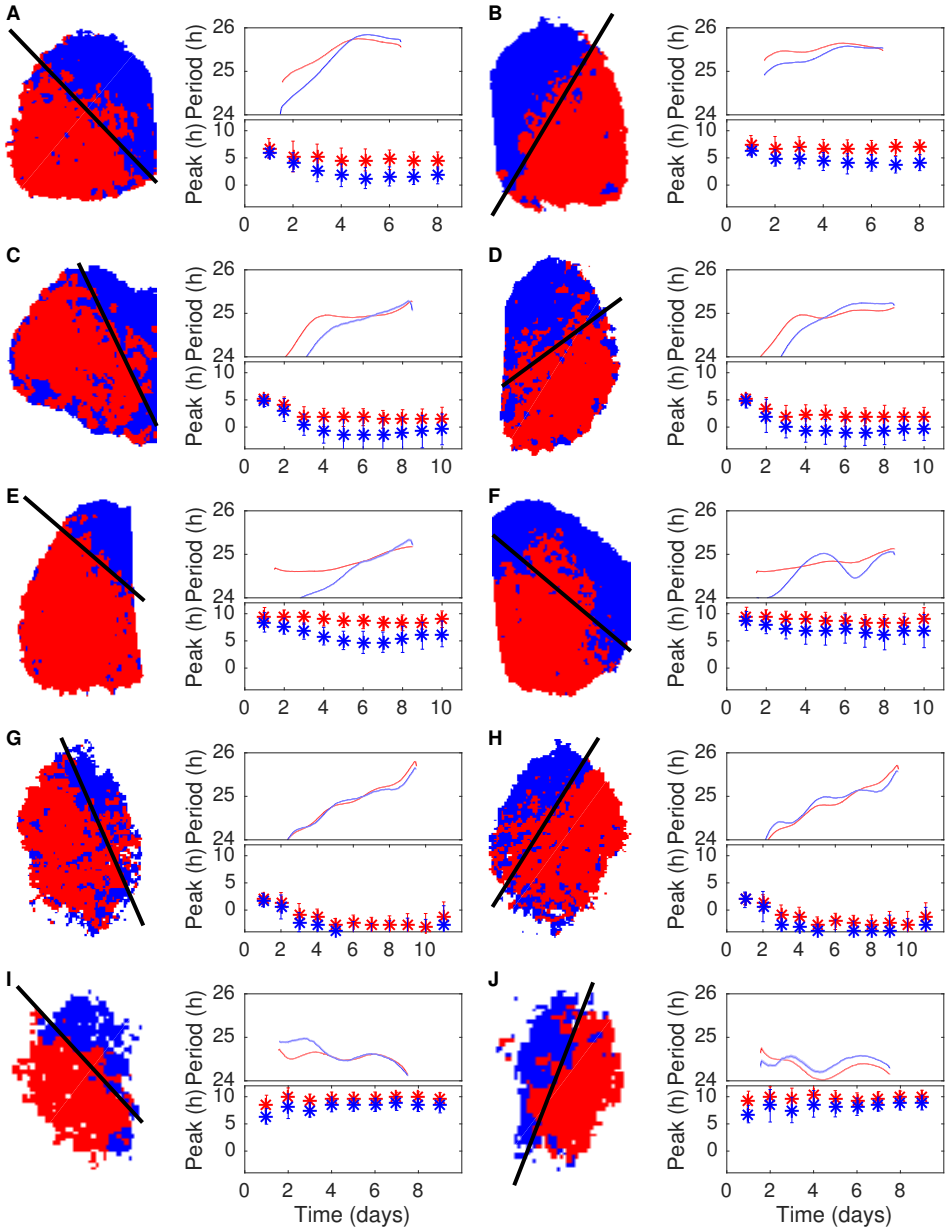


FIGURE S6. **Pixel-based clustering reveals that the period of oscillators in the ventrolateral region was longer and stabilized sooner than the period of oscillators in the dorsomedial region.** The clusters for five bilateral SCN (A, C, E, G, and I show the left nuclei and B, D, F, H and J show the right nuclei) consistently organized into similar spatial patterns after removal of TTX. Linear discriminant analysis (black line) separated each unilateral SCN into a ventrolateral and dorsomedial component. The mean period of each cluster and the mean (+/- SD) peak time of each cycle for the two identified clusters showed reproducible patterns across SCN. The mean period during day 3 in the ventral cluster (dark red) was longer than that of the dorsal (dark blue) cluster. The mean period of the dorsal cluster reached its stable value (within 15 minutes of its average period during day 6) before that of the ventral cluster, and on day 6, the mean peak time of the dorsal cluster led that of the ventral cluster.

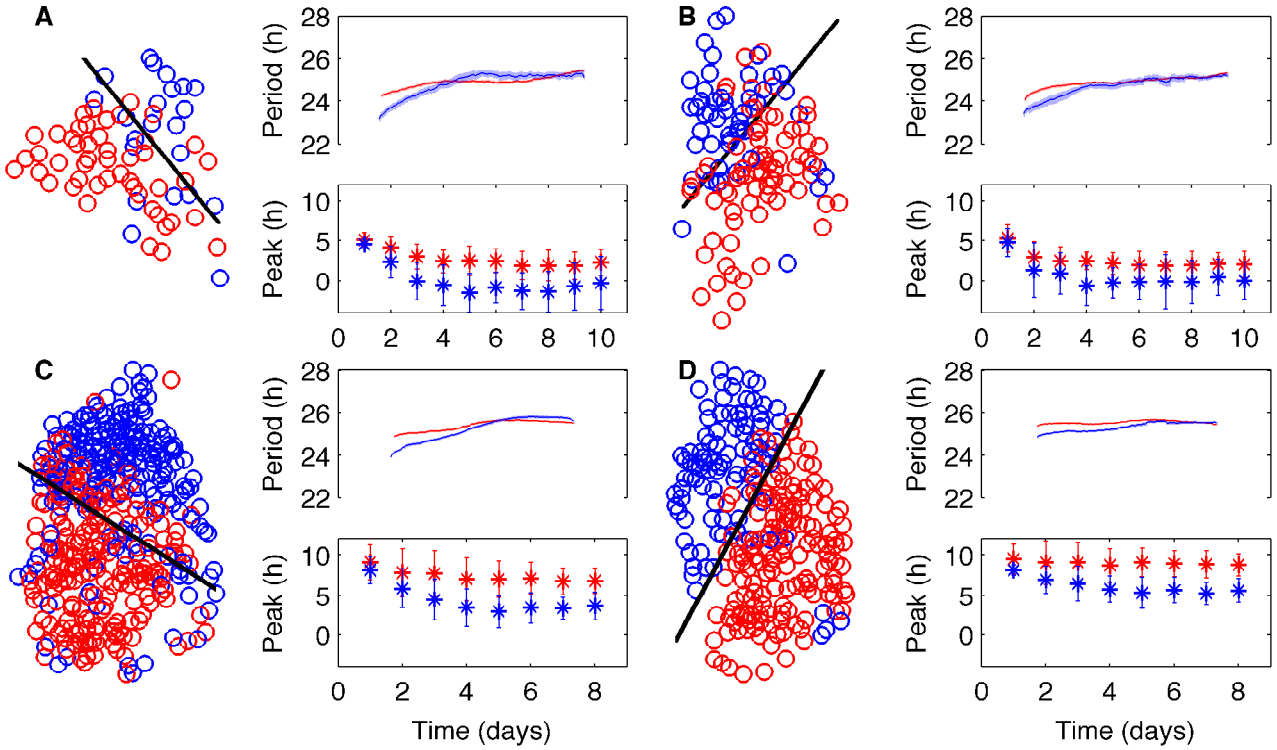


FIGURE S7. **Cell-based clustering reveals that the period of oscillators in the ventrolateral region was longer and stabilized sooner than the period of oscillators in the dorsomedial region.** The clusters for two bilateral SCN (A and C show the left nuclei and B and J show the right nuclei) consistently organized into similar spatial patterns after removal of TTX. Linear discriminant analysis (black line) separated each unilateral SCN into a ventrolateral and dorsomedial component. The mean period of each cluster and the mean (+/- SD) peak time of each cycle for the two identified clusters showed reproducible patterns across SCN. The mean period during day 3 in the ventral cluster (dark red) was longer than that of the dorsal (dark blue) cluster. The mean period of the dorsal cluster reached its stable value (within 15 minutes of its average period during day 6) before that of the ventral cluster, and on day 6, the mean peak time of the dorsal cluster led that of the ventral cluster.